Korean J. Chem. Eng., 38(4), 843-851 (2021)
DOI: 10.1007/s11814-020-0707-y

pISSN: 0256-1115
eISSN: 1975-7220

Forward osmosis process membranes incorporated with functionalized P.ZnO nanoparticles for organic fouling control

Rezvaneh Ramezani Darabi, Majid Peyravi, and Mohsen Jahanshahi†

Department of Chemical Engineering, Babol Noshirvani University of Technology, Shariati Ave., Babol, Iran, Post Code: 47148-71167
(*Received 17 May 2020 • Revised 16 October 2020 • Accepted 5 November 2020*)

Abstract−The incorporation of functional nanoparticles in polyamide (PA) membranes is an efficient procedure for the thin film nanocomposite (TFN) membranes development with enhanced desalination efficiency. Our aim was to synthesize forward osmosis process (FOP) membranes incorporated with PIP-functionalized ZnO (P.ZnO) nanoparticles, which were produced with surface functionalities groups of amine, epoxy and hydroxyl. The outcomes of FTIR confirmed the synthesis of P.ZnO nanoparticles, while WCA, AFM and FESEM supported the alterations in chemical and physical attributes of the FOP membranes surface upon P.ZnO nanoparticles incorporation. In both reverse osmosis process (ROP) and FOP tests, outcomes illustrated that the TFN-P.ZnO0.03 membrane was the most promising FOP and ROP membrane as it exhibited 119% higher pure water flux (PWF) (in FOP test) than the base FOP membrane. In terms of FOP membrane fouling propensity, the TFN-P.ZnO0.03 membrane also illustrated lower fouling propensity compared to the base membrane. Our outcomes have provided novel intuition into the structure-efficiency correlation of TFN FOP membranes and can be advantageous for the synthesis of the wide confinement of nanoparticles incorporated FOP membranes.

Keywords: Zinc Oxide Nanoparticle, Functionalization, Thin Film Composite Membrane, Forward Osmosis Process, Fouling

INTRODUCTION

Membrane processes (MP) hold striking promise in addressing the challenge of pure water scarcity [1-3]. Forward osmosis process (FOP), as an emerging MP technology, has been getting increasing consideration in many applications such as seawater desalination, water purification [4], wastewater reuse [5], sustainable power generation [6] and food processing [7]. However, FOP poses crucial challenges as fouling, internal concentration polarization (ICP) [8] and reverse salt diffusion (RSD), while novel draw solution (DS) and FOP membranes are still under development [8,9]. The ICP phenomenon is a considerable challenge in FOP that reduces FOP membrane performance [10]. In FOP, the ICP describes the attenuation of DS concentration inside the sublayer. ICP can reduce the efficient osmotic driving force (ODF) and outcomes in poor pure water flux (PWF) performance [11,12]. Also, MP fouling is another basic challenge affecting MP separation [13,14]. The interaction of membrane top surface with organic, inorganic colloidal, or microbial species leads to MP fouling. Acting through distinct mechanisms (pore blockage, bacterial growth, gel formation and adsorption) in MP fouling causes a diminution of PWF, membrane selectivity, and a beneficial lifetime of membranes. Given the amount of natural organic substances, proteins and polysaccharides in wastewater sullage and natural waters, organic fouling poses a substantial operational difficulty in reverse osmosis process (ROP) and FOP [15-18]. Adsorption of the dissolved organic substance on the polymeric membrane (PM) outcomes in the foulants layer constitution enhances the hydraulic insistence to pure water permeation. The layer of foulant can also outcome in cake-enhanced osmotic pressure, causing to lower ROP membrane selectivity and a decrement of the ODF in FOP [15,19,20]. In the recent decade, prosperity has been gained for the thin-film composite (TFC) FOP membrane fabrication that consists a top polyamide (PA) layer on a polymeric sublayer [5,21,22]. Compared to earlier descendant of FOP membranes (as cellulose tri-acetate), higher FOP PWF can be generally gained. However, TFC FOP membranes are more likely to foul compared to their cellulose tri-acetate counterparts [15,23,24]. Surfaces with increment hydrophilicity generally demonstrated decrement organic fouling propensity because of a hydration layer formation, which enables a steric and energetic obstacle against organic foulant adsorption [15,25]. Striking scrambles have been created to ameliorate the fouling insistence of TFC FOP membranes by either incorporation hydrophilic nanomaterials during FOP membrane produced via interfacial polymerization processes (IPP) or grafting hydrophilic nanomaterials on the FOP membrane surface [26]. Surface modification utilizing hydrophilic nanoparticles to impart fouling insistence to TFC FOP membranes has been actively studied. Accordingly, various nanoparticles, consisting carbon-based nanomaterials [27,28] and metal oxide nanoparticles [29,30], have been implemented to provide antifouling TFC membranes for FOP applications. Shen et al. in 2016 [28] synthesized new thin film nanocomposite (TFN) membranes utilizing a 1,3-diaminobenzene/Graphene oxide (MPD/GO) solution as the MPD aqueous phase. Their new TFN membranes basically illustrated higher PWF, lower

†To whom correspondence should be addressed.
E-mail: mmohse@yahoo.com

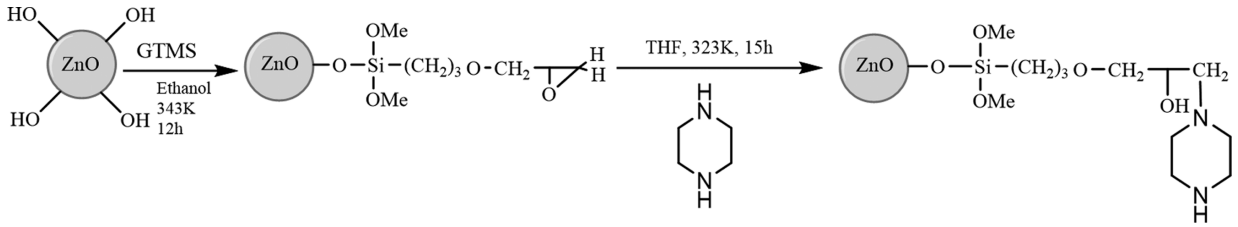

Scheme 1. P.ZnO nanoparticles synthesis.

S parameter, lower reverse salt flux (RSF) and higher NaCl salt rejection (SR) as compared to the bare TFC membrane. Also, their fouling experimental test represented that their TFN membranes sufficiently suppress the unfavorable fouling phenomenon, and their TFN membranes fouling was almost reversible. Zirehpour et al. in 2016 [31] incorporated metal organic framwork (MOF) nanoparticles into the cellulose triacetate (CTA) FOP membrane and improved its FOP performance in terms of NaCl salt selectivity and *S* parameter. Also, their new membrane extremely improved the CTA membrane antifouling attributes when compared to the bare FOP membrane. Faria et al. in 2017 [32] fabricated new anti-biofouling TFN membranes functionalized with GO-silver nanoparticles. Their outcomes showed that the utilization of GO-silver nanoparticles was an attractive and possible approach for the anti-biofouling development of TFN FOP membranes. In the current research, we introduced low-fouling amino-functionalized TFN FOP membranes via incorporation of modified inorganic nanoparticles into the top rejection layer through a synthesis of amino-functionalized zinc oxide (ZnO) nanoparticles. ZnO nanofiller is an excellent nanoparticle because of its high hydrophilicity, low price, chemical stability, environmentally friendly and non-toxic nature [33]. The hydroxyl groups of blank ZnO nanoparticles has made them superhydrophilic which can easily react with 3-Glycidyloxypropyl trimethoxysilane (GTMS) silane compound. GTMS-ZnO nanoparticle was subjected to reaction of amine functional piperazine (PIP) groups with ring-opening epoxy groups. These PIP-functionalized ZnO (P.ZnO) nanoparticles not only vary the reaction speed between MPD and trimesoyl chloride (TMC) monomers, but also affect the top PA layer morphology. With respect to FOP membrane efficiencies, we believe that the presence of such functionalized P.ZnO nanoparticles could significantly enhance TFC FOP membrane efficiency. The principal targets of our paper are to study the potential of P.ZnO nanoparticles as inorganic nanofillers in the top PA layer of TFC FOP membrane to reduce organic fouling and improve FOP membrane performance. To the authors' knowledge, modified ZnO nanoparticles, in particular utilizing functionalized P.ZnO nanoparticles, were not beforehand incorporated into the top PA layer of TFC FOP membranes and not even beforehand synthesized.

MATERIALS AND METHODS

1. P.ZnO Nanoparticles Synthesis

For producing ZnO nanofillers, solutions (A) and (B) were created conforming to the following manner: solution (A) contains 29.7 Zn $(NO_3)_2{\cdot}6H_2O$ (Merck) dissolved in 1 L pure water, and solution (B) contains 12.7 Na_2CO_3 (Merck) dissolved in 1 L water. Then two solutions were mixed together. The obtained mixture of the two solution was centrifuged and afterward rinsed with pure water. The white powder was dried at 373 K for 6 h after rinsing with acetone (Merck, ≥99.5%). Finally, obtained ZnO nanoparticles were calcined at 523 K for 2.5 h [34]. To synthesize GTMS (Sigma, ≥98%) grafted ZnO nanoparticles, 1 gr of produced ZnO nanoparticles and 2 ml GTMS dispersed in 50 ml ethanol (Merck, 96%) and produced solution were refluxed and stirred at 343 K overnight. After obtained product centrifugation, GTMS grafted ZnO were rinsed with ethanol and next dried in vacuum condition at 323 K for 24 h [35]. For modification of the GTMS grafted nanoparticle by PIP (Merck, ≥99.5%), 2 gr of the GTMS grafted ZnO nanoparticles and 6cc PIP compounds were added to 60 ml of tetrahydrofuran (THF, >95%) in a 200 ml of the flask and stirred for 15 h at 323 K. Then, the product was centrifuged and rinsed with a THF. The final products (P.ZnO) were dried for 24 h. The schematic preparation of P.ZnO nanoparticles is depicted in Scheme 1.

2. FOP Membranes

The sublayer was provided by the phase inversion technique (PIT) utilizing casting solution that was comprised of 14 wt% polyethersulfone (PES) (ultrason 6020), 2 wt% polyvinyl pyrrolidone (PVP, Sigma) and 84 wt% dimethylformamide (DMF, >99.8%, Merck), as represented in our previous paper [15,36]. To prepare the top PA layer, the membrane sublayer was immersed in a 2 wt% amine solution for 2 min and pulled up slowly with a rubber roller. Afterward, it was covered with a n-hexane solution layer containing 0.1 wt% TMC monomer. The produced FOP membrane was then heat-treated at 353 K for 5 min. TFN-P.ZnO membranes were synthesized identically as described, barring that various amounts of P.ZnO nanoparticles (0.01, 0.03 and 0.05 wt%) were dispersed in MPD amine solution. To obtain good P.ZnO dispersion, the mixtures of P.ZnO and MPD monomer solution were sonicated for 50 min at 296 K exactly before the IPP. The produced membranes incorporated with 0.01, 0.03, and 0.05 wt% of P.ZnO nanoparticles are noted as TFN-P.ZnO0.01, TFN-P.ZnO0.03 and TFN-P.ZnO0.05 membranes, respectively.

3. Characterization

The ZnO functional groups, GTMS-grafted ZnO, modified ZnO with PIP, were studied by ATR-FTIR (TENSOR 27, Germany). Cross-sectional and surface photograph of the bare TFC and P.ZnO.TFN0.03 membranes were imaged by utilizing a field emission scanning electron microscope (FESEM, Model: Mira 3-XMU) equipped with an energy-dispersive X-ray spectroscopy (EDX) unit. The water contact angle (WCA) of both base TFC and TFN-P.ZnO0.03 membranes was evaluated utilizing a WCA goniome-

ter (KRUSS BmbH, Germany). Characterization of the base TFC and TFN-P.ZnO membranes roughness was accomplished by an atomic force microscope (AFM model: Easyscan2 flex).

4. ROP Performance Evaluation

The TFC and TFN-P.ZnO membranes' intrinsic pure water permeability (PWP or A) and salt rejection (SR or R) were tested by an ROP cross-flow apparatus. The details of the cross-flow ROP setup and measurement manner were represented in our previous paper [15,36]. In brief, a FOP membrane (12.57 cm^2) was contacted to the 40 mM NaCl solution as a feed solution (FS) at an applied of 250 kpa to the PWF and SR measurement. The NaCl salt permeability coefficient (B, L/m^2 h) was calculated using Eq. (1).

$$B = J\left(\frac{1}{R} - 1\right) \quad (1)$$

where J is the PWF obtained for the 40 mM NaCl FS and 250 kpa applied pressure [4].

5. FOP Performance Evaluation

A lab-scale crossflow FOP apparatus was utilized in the PWF and RSF measurement as represented in our previous paper [36]. The FOP membrane cell (CF042- FO cell, Sterlitech) has an area of 38 cm^2. 2 M NaCl solution was utilized as DS while deionized water (DI) water was utilized as the FS. FS and DS were circulated utilizing two circular pumps with a constant cross-flow velocity of 800 mL/min. All FOP membranes were synthesized and tested in at least three measurements to yield an average value. Each testing was conducted for 1 hr and the temperature was 298±1.5 K during the FOP experiments. The FOP PWF (J_v) was measured by the FS weight change. The *S* parameter of the FOP membrane sublayer was specified by the B, A values (from ROP apparatus) and the PWF (from FOP apparatus) into Eq. (2) [8,36]:

$$J_v = \frac{D}{S}\left[\mathrm{Ln}\frac{A\pi_{draw} + B}{A\pi_{feed} + B + J_v}\right]$$

where D (m^2/s) is the NaCl diffusivity of the DS, and π_{draw} and π_{feed} are the DS and FS osmotic pressures.

Physically, the diffusion coefficient, D, represents the amount of solute which would diffuse across unit area in unit time under unit concentration gradient. In general, the diffusion coefficient is dependent on the type of salt and is constant for each salt. Hence, diffusion coefficient for NaCl at a constant concentration of 2 M is a constant value of 1.6×10^{-9} m^2/s [37,38].

6. FOP Fouling Experiments

FOP fouling experimental tests were accomplished with TFN-P.ZnO and base membranes by the laboratory FOP setup. The FS contained 350 mg/L sodium alginate dissolved in 10 mM NaCl. The FOP fouling experimental test was accomplished under the top active layer facing FS with 8.5 cm/s cross-flow velocities in both DS and FS channels. After loading an FOP membrane into FOP cell, a baseline experimental test was accomplished through a foulant-free FS (10 mM NaCl) to measure the PWF decline derived solely from DS dilution and reverse draw solute diffusion. The FOP fouling test was accomplished at the same initial PWF as the baseline experimental test. Then, fouling experimental test data were corrected to omit the PWF decline from DS dilution and reverse draw solute diffusion. Therefore, the presented data reflect only the PWF decline because of FOP membrane fouling. The baseline and FOP fouling experiments were accomplished in up to 8 hours [39].

RESULTS AND DISCUSSION

1. P. ZnO Nanoparticles

After ZnO nanoparticle synthesis through precipitation procedure, these were grafted with silane compounds by reaction between methoxy groups of GTMS and hydroxyl groups of ZnO nanoparticles. This reaction leads to graft GTMS silane compounds with the free head of the epoxy group on the ZnO nanoparticles. Ring-opening reaction of the epoxy was performed by a reaction between the amine groups of PIP with grafted ZnO nanoparticle, which leads to creating hydroxyl groups. The PIP monomer not only reacts with the epoxy through ring opening reaction with high activity but also amino groups of PIP modified make ZnO nanoparticles more hydrophilic and that can play a considerable role in FOP membrane performance. The papers even though employed PIP monomer for epoxy ring opening reaction in order to the exploration of PIP monomer reaction with the epoxy ring of GTMS-ZnO and incorporation of P.ZnO nanoparticles onto sublayer for FOP applications. IR spectroscopy was utilized to verify the produced ZnO nanoparticle chemical structure and the interaction of ZnO nanoparticle with GTMS and PIP. The FT-IR spectra of (a) ZnO nanoparticles, (b) GTMS-grafted ZnO nanoparticles and (c) the modified ZnO with PIP are demonstrated in Fig. 1. The wide peak between 3,300 cm^{-1} and 3,400 cm^{-1} relates to the ZnO nanoparticle hydroxyl groups. The peaks at 833, 1,045 and 2,900 cm^{-1} were imputed to Zn-O-Si, Si-O and methylene groups on the GTMS-grafted ZnO nanoparticles surfaces, respectively. The peak at 845 can be allocated to the epoxy stretching bond. For P.ZnO nanoparticle, a peak at about 3,440 cm^{-1} relates to the NH band that is overlapped with the hydroxyl stretching band formed by ring-opening reaction of the epoxy group.

2. TFC and TFN-P.ZnO Membranes Characterization

The presence of P.ZnO nanoparticles in the rejection PA layer was supported by EDX results indicated in Fig. 2 in which Zn element was identified on the PA top surface of TFN-P.ZnO membrane.

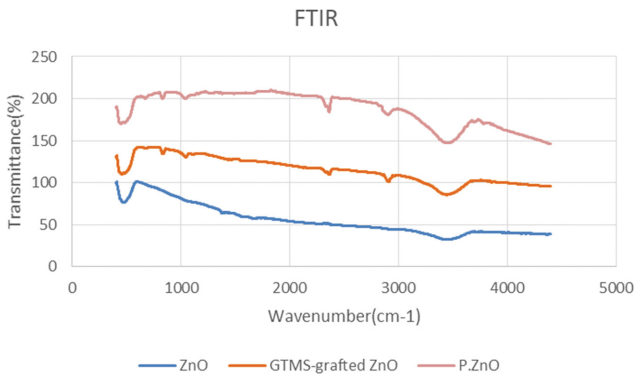

Fig. 1. FT-IR pattern of ZnO nanoparticles, GTMS-grafted ZnO nanoparticles, P.ZnO nanoparticles.

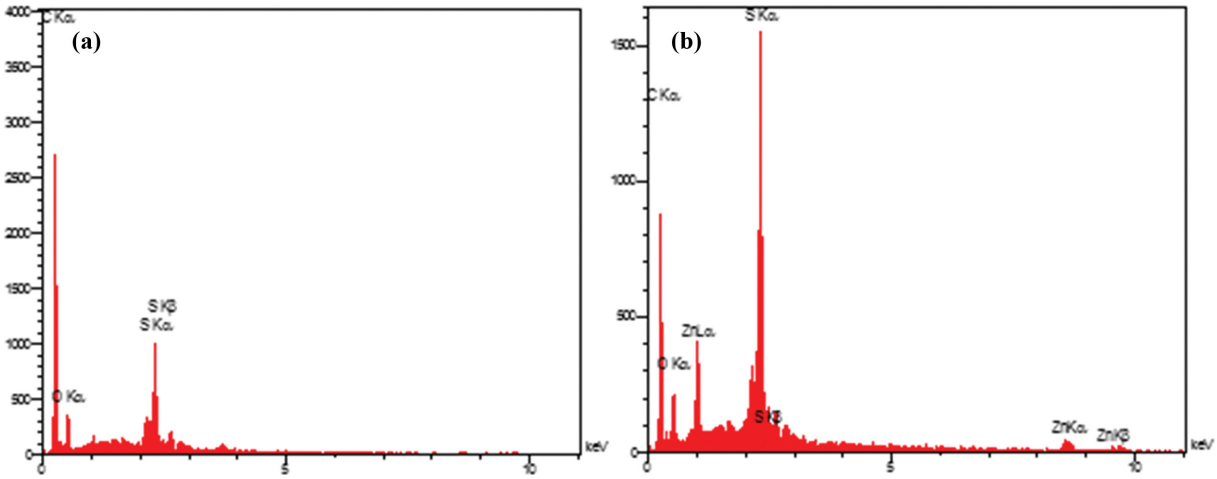

Fig. 2. EDX analysis of (a) base FOP membrane and (b) TFN-P.ZnO0.03 membrane.

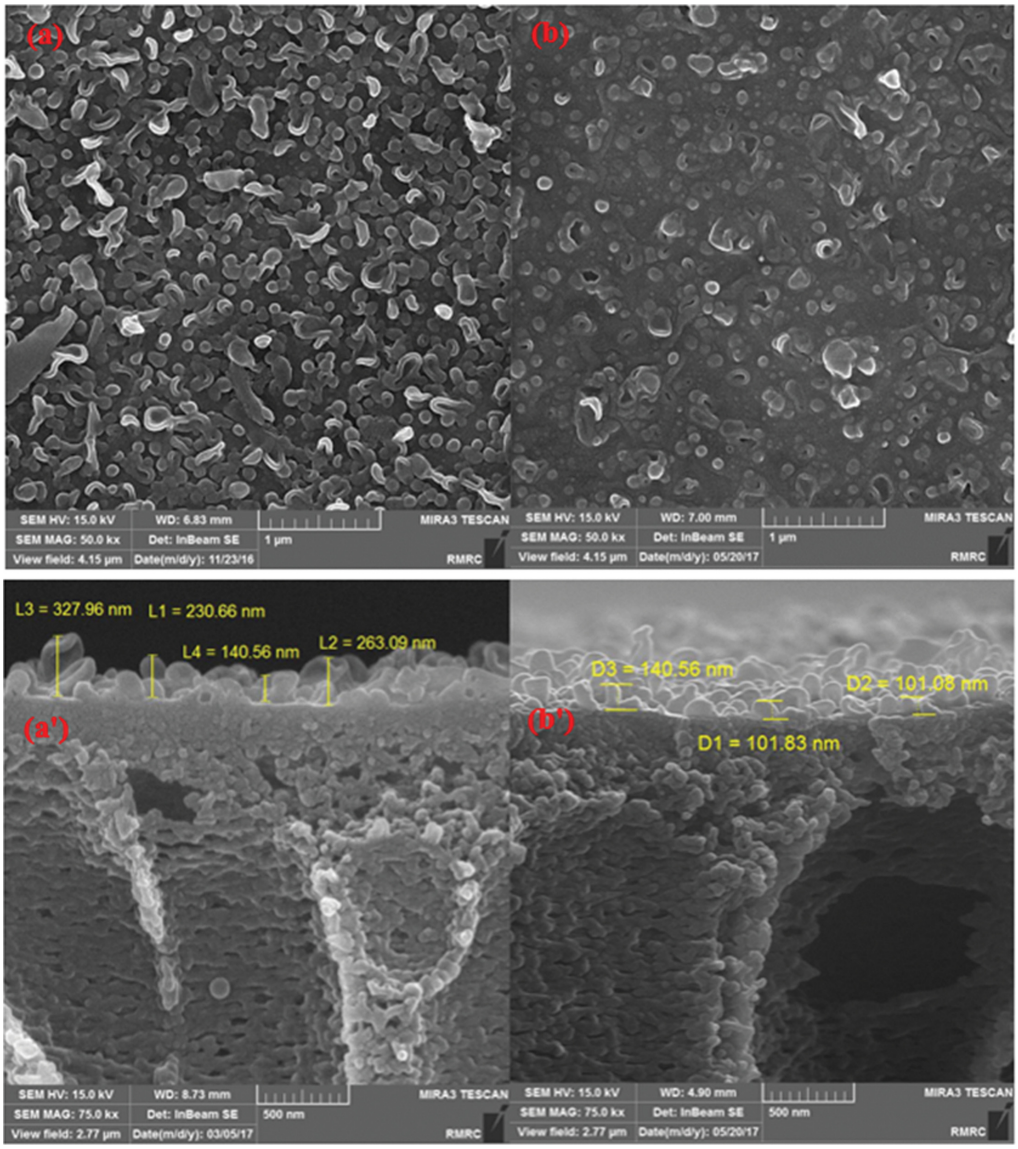

Fig. 3. FESEM photographs of the top surface and cross section FOP membranes: (a) TFC membrane top surface, (b) TFN-P.ZnO membrane top surface, (a') TFC membrane cross section, and (b') TFN-P.ZnO membrane cross section.

Fig. 3 demonstrates the surface and cross-section photo of the base TFC and TFN-P.ZnO membranes prepared by IPP between MPD and TMC. As seen, the base TFC membrane surface has "ridge and valley type" morphology, whereas this morphology was discounted and changed to "nodular" morphology for TFN-P.ZnO membrane. Regarding COCl groups of TMC organic monomer and NH_2 groups of MPD amine monomer [40], TMC is less soluble in pure water and the IPP mainly was accomplished in the organic phase. So to react with TMC monomer, migration of amine monomers to the TMC organic phase is required. The MPD amine migration is frequently governed by simple diffusion and convection. This rapid diffusion can form the ridge and valley type structure and the low diffusion can form the nodular structure. As illustrated by Solomon et al., the diffusion rate decrement of MPD monomers during IPP is one of the reasons for the nodular type PA formation [41-43]. Maybe, it was because the P.ZnO nanoparticles which possessed slower amine diffusion rate retarded the MPD molecules to diffuse from MPD aqueous phase to TMC organic phase by a steric barrier, consequently leading to the deceleration of IPP reaction. Thus, the wrinkle structure formation in TFN-P.ZnO membrane partially was as a result of the reaction between the amine of P.ZnO and MPD with TMC monomer during the IPP. Also, oxygen-containing groups in P.ZnO can theoretically interact with the TMC acylchloride groups, hence affecting the reaction speed between of two monomers. As such, the PA rejection layer formation was considerably affected by the loading of P.ZnO, which resulted in the varied surface morphology of the P.ZnO modified TFC membranes. Apart from the nodular structure formation, the TFN-P.ZnO membrane tended to have rougher top polyamide surface than the base TFC membrane containing P.ZnO nanoparticles. As seen, the addition of P.ZnO nanoparticles considerably reduced the rejection layer thickness. Compared to the base FOP membrane, there is a barrier efficacy of P.ZnO nanoparticles to the diffusivity of amine monomer from the aqueous MPD amine phase to reach to the interface of two monomers in the TMC organic phase, resulting in a thinner PA skin layer. Such a decrement in the PA top layer thickness remarkably lowered the mass transfer insistence, thereby enhancing the PWF [44].

The average WCAs measured on base and amino-functionalized TFN-P.ZnO membranes surface are illustrated in Table 1. The base polyamide FOP membrane has a WCA of 51.15°, which is higher than of TFN-P.ZnO membranes. Aromatic rings are the predominant functional groups in the base polyamide; these aromatic rings cannot form hydrogen bonds with pure water molecules and so contribute to the high WCA observed in the base TFC membrane. TFN-P.ZnO membranes exhibit more hydrophilicity among synthesized TFN membranes due to the existence of P.ZnO nanoparticles in the top PA surfaces. The WCA could be affected by membrane surface roughness. The roughness parameters of the base TFC and TFN-P.ZnO membranes are summarized in Table 1 in terms of the average surface roughness (Sa), the mean square roughness (Sq) and the mean height difference between the peaks and valleys (Sy). As demonstrated, the average parameters of roughness were enhanced by adding P.ZnO nanoparticles. As represented in Table 1, by adding 0.01, 0.03 and 0.05 wt% P.ZnO nanoparticles in the rejection PA layer, WCAs were reduced to 48.56°, 44.30° and 42.54°, respectively. To eliminate the efficacy of roughness on apparent WCA, the corrected WCA (θ') just correlated to the nature of FOP membrane materials were utilized to specify the FOP membrane surface hydrophilicity, which was determined by $\cos\theta' = \cos\theta/r$, where r parameter was surface roughness area proportion corresponding to the proportion of the TFC membrane surface area to the TFC membrane projected area acquired by AFM [45]. As demonstrated in Table 1, the corrected WCA of base TFC membrane was around 54.72°. After loading of 0.01, 0.03 and 0.05 wt% P.ZnO nanoparticles, the corrected WCAs decreased to 50.75°, 45.91° and 44.50°, respectively. The variation of corrected WCA suggested that the top surface hydrophilicity of FOP membranes could be tuned by loading of P.ZnO nanoparticles during IPP. This enhancement in TFN-P.ZnO membrane hydrophilicity can be imputed to the following sakes. First, the hydroxyl groups resulting from the opening reaction of the epoxy ring in the P.ZnO nanoparticles surface can form a hydrogen bond with the molecules of water to increase the TFN-P.ZnO membrane hydrophilicity. Secondly, adding P.ZnO nanoparticles may disrupt the IPP through a reaction between acyl chloride groups (remained on the TMC surface without reacting with MPD amine groups) with hydroxyl groups from the opening reaction of the P.ZnO nanoparticles epoxy ring. This reaction produces carboxyl acid groups that further enhances the TFN-P.ZnO membranes hydrophilicity. Thus, there was a striking increment in the TFN-P.ZnO membrane hydrophilicity, and this enhancement was envisaged due to the hydrophilic functional groups (hydroxyl, amine and epoxy) of P.ZnO nanoparticles. A hydrophilic TFN-P.ZnO membrane surface facilitates water molecule uptake onto TFN-P.ZnO membrane surface, which enhances the PWP.

3. TFC and TFN-P.ZnO Membranes Intrinsic Properties

The effects of P.ZnO concentration in the reactive MPD amine solution during FOP membrane formation on the PWP and SR of the TFC membranes are indicated in Table 2. As demonstrated, the PWP increased considerably from 2.26 L/m^2·h·bar of base TFC membrane to 5.46 L/m^2·h·bar of TFN-P.ZnO0.05 membrane. This

Table 1. Effect of P.ZnO nanoparticles on the properties of FOP membrane with respect to WCA, Corrected WCA, *S* parameter and Roughness

Membrane	WCA	r Parameter	Corrected WCA	*S* parameter (mm)	Roughness		
					Sa (nm)	S_q (nm)	S_y (nm)
TFC	51.15°	1.086	54.72°	0.586±0.04	55.85	68.68	375.57
TFN-P.ZnO0.01	48.56	1.046	50.75	0.374±0.03	78.92	107.88	731.31
TFN-P.ZnO0.03	44.30°	1.029	45.91°	0.262±0.02	86.86	108.86	822.52
TFN-P.ZnO0.05	42.54	1.033	44.50	0.241±0.04	88.46	111.48	907.91

Table 2. Separation properties of FOP membranes.

Membranes	Water permeability (L/m^2 h bar)	Water permeability A ($\times10^{-12}$ m/s Pa)	Salt rejection (%)	Salt permeability B ($\times10^{-8}$ m/s)
TFC	2.26±0.19	6.28±0.34	95.87±1.43	6.76±0.31
TFN-P.ZnO0.01	3.54±0.21	9.83±0.37	94.99±1.40	12.96±0.41
TFN-P.ZnO0.03	4.71±0.27	13.08±0.41	93.98±1.40	20.95±0.44
TFN-P.ZnO0.05	5.46±0.31	15.17±0.43	91.22±1.36	36.49±0.49

Table 3. Comparison of FOP performance with literature data

Membranes	Water flux (L/m^2 h) FOP	Reverse salt flux (g/m^2 h) FOP	J_s/J_w (g/L)	Feed solution	Draw solution	References
TFC	22.14±0.74	7.21±0.46	0.326	10 mM NaCl	2 M NaCl	In this work
P.ZnO-TFN0.01	34.67±0.76	8.35±0.47	0.241	10 mM NaCl	2 M NaCl	In this work
P.ZnO-TFN0.03	48.46±0.81	9.41±0.48	0.194	10 mM NaCl	2 M NaCl	In this work
P.ZnO-TFN0.05	53.76±0.82	13.41±0.48	0.249	10 mM NaCl	2 M NaCl	In this work
0.5MWfT/M-P	20.3	13.3	0.66	DI water	2 M NaCl	[9]
Modified-TFC	30	9	0.3	DI water	1.5 M NaCl	[11]
PGO-FO-5	14.18	-	1.05	10 mM NaCl	2 M NaCl	[46]
TFC 21	17.0±0.9	46	2.7	DI water	2 M NaCl	[47]
MPD/TAEA+TMC	26.9	9.3	0.35	DI water	2 M NaCl	[48]

enhancement of PWP can be elucidated as follows. (1) The incorporation of P.ZnO in the thin top PA layer enhanced the FOP membrane hydrophilicity, which can attract pure water molecules into the TFN-P.ZnO membrane matrix and facilitates TFN-P.ZnO membrane transport. (2) Increase in the top PA surface area that FS was in contact with a surface area as an outcome of the nodular structure formation. (3) The presence of the voids at the interface between embedded P.ZnO and PA matrix provided water flow channels and also simple diffusion through the top PA matrix. (4) The special area between P.ZnO nanoparticles and PA chains, constructed extra free volume in PA layer and thus prepared a further path for water transport. (5) The incorporation of P.ZnO reduced the TFN-P.ZnO membrane rejection layer thickness, contributing to a lower insistence of transport and enhanced PWP. Many researchers have shown that using hydrophilic nanoparticles or the attachment of hydrophilic groups on nanoparticles surface leads to the reduction in nanoparticle agglomeration and better distribution of nanoparticles on the membrane surface [46, 47]. For example, Gong et al. demonstrated that the good dispersity and better distribution of UIO-66-NH_2 nanoparticles in aqueous solution is owing to the abundant hydrophilic amine groups in the UIO-66-NH_2 nanoparticles [47]. It seems that the amine group of P.ZnO nanoparticles can lead to the proper dispersity of nanoparticles, reduction in nanoparticles agglomeration and better distribution of nanoparticles on the surface. Thus, the hydrophilic groups of P.ZnO nanoparticles form a very weak linkage with the MPD monomer, which reduces nanoparticle agglomeration at the FOP membrane surface and increases the PWP. Although porosity is a major parameter for the enhancement of the water flux in FOP, it should be noted that only utilizing nanoparticles in the support layer, not in the polyamide layer, leads to increase the porosity. Since, in the current work, P.ZnO nanoparticles have been used in the polyamide layer, and generally the polyamide layer is a dense layer and the porosity is not considered for it [48], so the application of P.ZnO nanoparticles cannot change the TFN membrane porosity.

In separation efficiency terms, we found that the SR decreased insignificantly by adding P.ZnO nanoparticles until 0.03 wt% from 95.87% base TFC to 93.98% of TFN-P.ZnO0.03 membrane and decreased further for TFN-P.ZnO0.05 to 91.22. This can be explained as follows. (1) SR by nodular structure was decreased because of more open morphology of nodular structure in analogy to ridge and valley structure. (2) SR by the void space between P.ZnO and top PA matrix is low as the outcome of the large sizes of the channel. (3) SR by the lower rejection layer thickness is low because of lower transport resistance [23,28,49,50]. This explanation can be better supported by the TFN-P.ZnO0.03 membrane FESEM image information. While maintaining high SR, TFN-P.ZnO0.03 was able to provide 108% more PWP compared to the base TFC. Therefore, TFN-P.ZnO0.03 was chosen for further fouling evaluation.

4. TFC and TFN-P.ZnO Membranes Performance in FOP

Table 3 demonstrates the FOP performance of the base TFC membrane with different P.ZnO loadings. The PWF increased for TFN-P.ZnO membranes from 22.14 of the base TFC membrane to 34.67, 48.46 and 53.76 for TFN-P.ZnO0.01, TFN-P.ZnO0.03 and TFN-P.ZnO0.05 membranes, respectively. It indicates that the PWF of all TFN-P.ZnO membranes was higher than the base TFC membrane. The PWF increased remarkably with the increment in the P.ZnO loading, illustrating an identical tendency with that of the PWP indicated in Table 2. Similarly, this increment in PWF should be imputed to the combined efficacy of the thinner top PA layer, additional passages formed, enhanced hydrophilicity, etc., as mentioned in section 3.2. Another substantial index of the FOP membranes, the *S* value, is illustrated in Table 1. Generally, P.ZnO-

incorporated membranes with higher PWF have lower *S* parameters, ascribed to their less ICP effect and higher hydrophilicity. This trend for RSF is agreeing with the behavior for SR, i.e., a higher SR indicates a lower RSF [36]. However, the RSF enhances a little up to 0.03 wt% P.ZnO loading and then enhances further with higher P.ZnO loading to 0.05 wt% in the top PA layer, which was in accommodation with the tendency of the SR change. Therefore, P.ZnO loading of 0.03 wt% in the top PA rejection layer was the optimal incorporation of P.ZnO nanoparticles to produce promising FOP membranes. Interestingly, although the RSF enhancement of TFN-P.ZnO0.03 membrane was moderate when contrasted with the benchmark in this paper, the RSF of TFN-P.ZnO0.03 membrane was lower than (or almost equal) TFC and TFN membranes in the literature (indicate Table 3) [9,11,51-53], connoting that an approximately defect-free PA layer is produced after loading of P.ZnO nanoparticles. Also, the RSF/PWF ratio of all membranes is illustrated in Table 3. A small RSF/PWF usually demonstrates a higher FOP selectivity. Membrane selectivity was decreased when P.ZnO nanoparticles were incorporated into the TFC membrane. The slight decrement of RSF/PWF value for TFN-P.ZnO0.03 may be as an outcome of the non-selective voids formed at the PA layer interface, where NaCl salt can permeate with lower resistance. Nevertheless, RSF/PWF of TFN-P.ZnO0.03 membrane is much smaller than most other TFN membrane loading with other fillers, such as GO, $CaCO_3$, carbon-TiO_2 composites, and GO-TiO_2 composite. In summary, the high PWF, low RSF and small RSF/PWF attained utilizing TFN-P.ZnO0.03 membrane proposes that the loading of P.ZnO nanoparticles was a beneficial approach to optimize the TFC membrane of FOP performance. To provide a beneficial analogy, the FOP performance of the homemade membranes was contrasted with other FOP membranes studied in the other literature as demonstrated in Table 3. Compared to other reported results, TFN-P.ZnO0.03 membrane has presented superior PWF while maintaining relatively high SR and selectivity. The current paper shows that P.ZnO presents considerable advantages over other fillers in the PA rejection layer in high PWF and controlling the salt reverse diffusion.

5. Organic Fouling of TFC and TFN-P.ZnO Membranes

Since the membrane fouling experiments for FOP were accomplished in batch mode, the ODF for PWF kept decreasing due to the concentration of FS and dilution of DS. Therefore, the PWF decrement in the fouling experimental tests was created by FOP membrane fouling as well as the decrement in the ODF. So, a baseline experimental test is essential for FOP fouling tests to isolate the efficacy of FOP membrane fouling. For instance, baseline tests can counteract the impression of FOP fouling and the decrement of ODF as an outcome of the FS concentration and the dilution of DS. Furthermore, the outcomes from the baseline experimental tests can be utilized to appraise the efficacy of DS dilution and ICP phenomenon on FOP performance [54]. To separate the effects of membrane fouling and decrease of ODF, the corrected normalized water flux instead of the actual observed water flux was used for the water flux decline curves from the fouling tests presented in the current work. To calculate normalized water flux, the base-

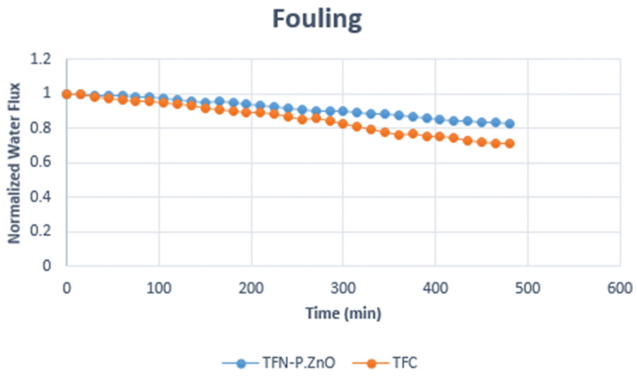

Fig. 4. Normalized PWF of base TFC and TFN-P.ZnO0.03 membranes as a function of time.

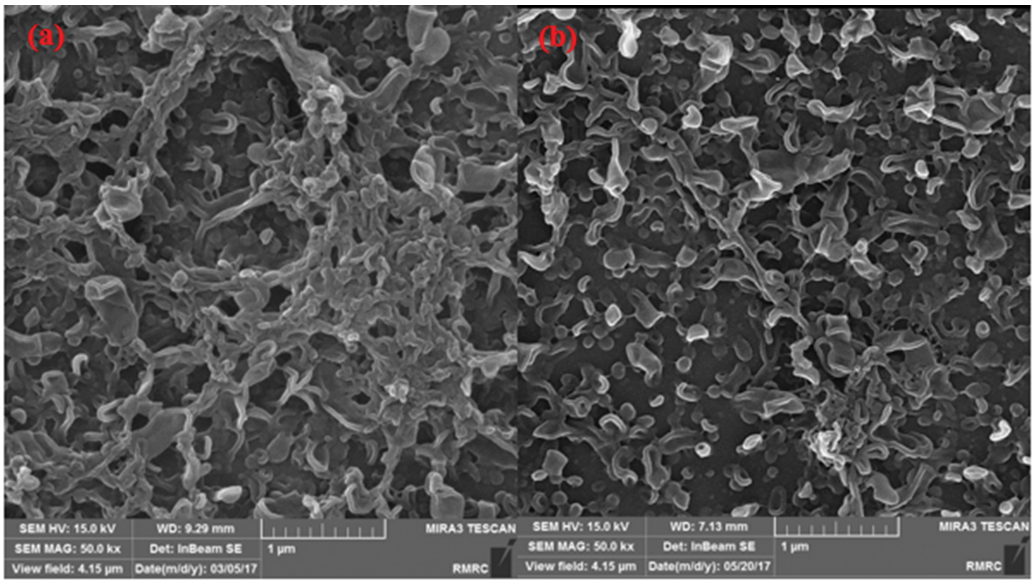

Fig. 5. FESEM images of FOP membranes after fouling: (a) base TFC membrane, (b) TFN-P.ZnO0.03 membrane.

line flux was divided by its corresponding initial water flux [54]. Hence, the flux decline curves demonstrated in Fig. 4 solely represent the effect of membrane fouling. Also, in the current research, alginate was elected as a model foulant to demonstrate polysaccharides abundant in wastewater. The alginate concentration in the FS, 350 mg/L, is remarkably higher than the alginate concentration in fouling investigations [15,25]. Outcomes in the literature have shown that alginate leads to substantial fouling and PWF reduction in FOP membranes [25,28]. The reverse diffusion of DS to the FS causes NaCl salts accumulated area at the PA layer and FS stream interface. This phenomenon decreases the efficient ODF, and hence the loss of the FOP water flux. Alginate layer that hoard on the FOP membrane surface intensifies the efficacy through cake-enhanced osmotic pressure. This is while the FOP membrane surface attributes can exacerbate or alleviate the FOP fouling propensity. Hydrophilic membrane surface can provide efficient alterations on the FOP membrane top PA surface interaction with foulants. The thin film of pure water molecules that forms on a surface of hydrophilic FOP membranes through hydrogen bonding hampers deposition of foulants and hence creates a lower FOP membrane fouling propensity. As shown in Figs. 4 and 5, the PWF decline of TFN-P.ZnO0.03 membrane with time is much slower than of the base TFC membrane, proposing lower FOP fouling tendency. At the end of the FOP fouling test, the PWF of TFN-P.ZnO0.03 decreased to 17% of its initial PWF, while that of base TFC was 29%. This lower FOP fouling propensity offered that a discontinuous and/or thinner alginate layer is exhibited on the TFN-P.ZnO0.03 membrane surface. For TFN membranes with a hydrophilic top surface, the molecules of water can comfortably adhere to the hydrophilic top surface via hydrogen bonding, eventually creating a thin boundary layer of pure water between the bulk solution and FOP membrane, which serves as a hindrance to restrain unfavorable adhesion of hydrophobic foulants [48].

CONCLUSION

Self-synthesized ZnO nanoparticles were effectively modified by epoxy and piperazine amine to produce amino functionalized ZnO nanoparticles, termed as P.ZnO nanoparticles. The TFN membranes were then produced by a varied amount of P.ZnO nanoparticles loading (in the range of 0.01-0.05 wt%) into the PA top layer. Our paper considers the interactions between P.ZnO nanoparticles and the PA top rejection layers, and looks at P.ZnO nanoparticle efficacy on the physicochemical attributes and the ROP and FOP efficiency of the constructed membranes. The top surface morphology and thickness of the PA film are strikingly altered with the introduction of P.ZnO nanoparticles. The variation in thickness reversely correlates with the increased PWF and is an outcome of the slow MPD amine monomer diffusion rate to the organic phase. The PWF was remarkably improved by approximate 119% utilizing TFN-P.ZnO0.03 membrane while the RSF changed insignificantly. Outcomes also illustrated that TFN-P.ZnO0.03 demonstrated a lower degree of PWF decrement compared to the base FOP membrane when sodium alginate was employed as a fouling agent. These findings corroborated the positive efficacy of P.ZnO incorporation in FOP membranes on fouling mitigation.

ACKNOWLEDGEMENT

The authors acknowledge the funding support of Babol Noshirvani University of Technology through Grant program No. BNUT/389026/99.

NOMENCLATURE

MP : membrane processes
FOP : forward osmosis process
Icp : internal concentration polarization
RSD : reverse salt diffusion
DS : draw solution
ODF : osmotic driving force
PWF : pure water flux
ROP : reverse osmosis process
PM : polymeric membrane
TFC : thin-film composite
PA : polyamide
IPP : interfacial polymerization processes
TFN : thin film nanocomposite
MPD/GO : 1,3-diaminobenzene/graphene oxide
RSF : reverse salt flux
SR : salt rejection
MOF : metal organic framwork
CTA : cellulose triacetate
ZnO : zinc oxide
GTMS : 3-glycidyloxypropyl trimethoxysilane
PIP : piperazine
P.ZnO : PIP-functionalized ZnO
TMC : trimesoyl chloride
THF : tetrahydrofuran
PIT : phase inversion technique
PES : polyethersulfone
PVP : polyvinyl pyrrolidone
DMF : dimethylformamide
FESEM : field emission scanning electron microscope
EDX : energy-dispersive X-ray spectroscopy
WCA : water contact angle
AFM : atomic force microscope
FS : feed solution
DI : deionized water

REFERENCES

1. A. Rahimpour, M. Jahanshahi and M. Peyravi, *J. Environ. Health Sci.*, **12**, 55 (2014).
2. M. Peyravi, A. Rahimpour, M. Jahanshahi, A. Javadi and A. Shockravi, *Micropor. Mesopor. Mater.*, **160**, 114 (2012).
3. H. Hoseinpour, M. Peyravi, A. Nozad and M. Jahanshahi, *J. Taiwan Inst. Chem. Engrs.*, **67**, 453 (2016).
4. M. Arjmandi, M. P. Chenar, M. Peyravi and M. Jahanshahi, *J. Inorg. Organomet. Polym.*, **29**, 178 (2019).
5. X. Zhang, J. Tian, Sh. Gao, Zh. Zhang, F. Cui and Ch. Y. Tang, *J. Membr. Sci.*, **527**, 26 (2017).
6. N. Y. Yip, A. Tiraferri, W. A. Phillip, J. D. Schiffman, L. A. Hoover,

Y. Ch. Kim and M. Elimelech, *Environ. Sci. Technol.*, **45**, 4360 (2011).
7. N. K. Rastogi, *Crit. Rev. Food Sci. Nutr.*, **56**, 266 (2016).
8. N. Niksefat, M. Jahanshahi and A. Rahimpour, *Desalination*, **343**, 140 (2014).
9. S. Mansouri, S. Khalili, M. Peyravi, M. Jahanshahi, R. R. Darabi, F. Ardeshiri and A. S. Rad, *Korean J. Chem. Eng.*, **35**, 2256 (2018).
10. Z. Dabaghian, A. Rahimpour and M. Jahanshahi, *Desalination*, **381**, 117 (2016).
11. L. Huang, J. T. Arena and J. R. McCutcheon, *J. Membr. Sci.*, **499**, 352 (2016).
12. R. R. Darabi, M. Peyravi and M. Jahanshahi, *Chem. Eng. Res. Des.*, **145**, 85 (2019).
13. M. Khajouei, M. Peyravi and M. Jahanshahi, *J. Membr. Sci.*, **3**, 2 (2017).
14. M. Peyravi, A. Rahimpour and M. Jahanshahi, *J. Membr. Sci.*, **473**, 72 (2015).
15. R. R. Darabi, M. Jahanshahi and M. Peyravi, *Chem. Eng. Res. Des.*, **133**, 11 (2018).
16. M. Khajouei, M. Jahanshahi, M. Peyravi, H. Hoseinpour and A. S. Rad, *Chem. Eng. Res. Des.*, **117**, 287 (2017).
17. M. Kazemi, M. Jahanshahi and M. Peyravi, *Carbohydr. Polym.*, **198**, 164 (2018).
18. A. S. Rad, D. Zareyee, M. Peyravi and M. Jahanshahi, *Appl. Surf. Sci.*, **390**, 444 (2016).
19. M. Kazemi, M. Jahanshahi and M. Peyravi, *J. Hazard. Mater.*, **344**, 12 (2018).
20. Y. Kim, M. Elimelech, H. K. Shon and S. Hong, *J. Membr. Sci.*, **460**, 206 (2014).
21. F. Esfandian, M. Peyravi, A. A. Ghoreyshi, M. Jahanshahi and A. S. Rad, *Arab. J. Chem.*, **12**, 5325 (2017).
22. M. Peyravi, A. Rahimpour and M. Jahanshahi, *J. Membr. Sci.*, **423**, 225 (2012).
23. M. Peyravi, M. Jahanshahi, A. Rahimpour, A. Javadi and S. Hajavi, *Chem. Eng. J.*, **241**, 155 (2014).
24. E. Jannatduost, A. A. Babaluo, F. Abbasi, M. A. Ardestani and M. Peyravi, *Desalination*, **250**, 1136 (2010).
25. N. Shafaei, M. Jahanshahi, M. Peyravi and Q. Najafpour, *Korean J Chem Eng.*, **33**, 2968 (2016).
26. R. Zhang, Y. Liu, M. He, Y. Su, X. Zhao, M. Elimelech and Z. Jiang, *Chem. Soc. Rev.*, **45**, 5888 (2016).
27. Z. Dabaghian and A. Rahimpour, *Chem. Eng. Res. Des.*, **104**, 647 (2015).
28. L. Shen, S. Xiong and Y. Wang, *Chem. Eng. Sci.*, **143**, 194 (2016).
29. D. Emadzadeh, W. J. Lau, M. Rahbari-Sisakht, H. Ilbeygi, D. Rana, T. Matsuura and A. F. Ismail, *Chem. Eng. J.*, **281**, 243 (2015).
30. A. Tiraferri, Y. Kang, E. P. Giannelis and M. Elimelech, *Environ. Sci. Technol.*, **46**, 11135 (2012).
31. A. Zirehpour, A. Rahimpour, S. Khoshhal, M. D. Firouzjaei and A. A. Ghoreyshi, *RSC Adv.*, **6**, 70174 (2016).
32. A. F. Andreia, C. Liu, M. Xie, F. Perreault, L. D. Nghiem, J. Ma and M. Elimelech, *J. Membr. Sci.*, **525**, 146 (2017).
33. X. Feng, H. Guo, K. Patel, H. Zhou and X. Lou, *Chem. Eng. J.*, **244**, 327 (2014).
34. M. Abbasian, N. K. Aali and S. E. Shoja, *J. Macromol. Sci. A.*, **50**, 966 (2013).
35. P. Liu and T. Wang, *Curr. Appl. Phys.*, **8**, 66 (2008).
36. R. R. Darabi, M. Peyravi, M. Jahanshahi and A. A. Qhoreyshi, *Korean J. Chem. Eng.*, **34**, 2311 (2017).
37. E. A. Guggenheim, *J. Chem. Soc. Faraday Trans*, **50**, 1048 (1954).
38. J. E. Burkell and J. W. T. Spinks, *Can. J. Chem.*, **30**, 311 (1952).
39. Y. Liu and B. Mi, *J. Membr. Sci.*, **407**, 136 (2012).
40. M. Zargar, Y. Hartanto, B. Jin and S. Dai, *J. Membr. Sci.*, **521**, 53 (2017).
41. D. Ma, S. B. Peh, G. Han and S. B. Chen, *ACS Appl. Mater.*, **8**, 7523 (2017).
42. Y. Li, Y. Su, Y. Dong, X. Zhao, Z. Jiang, R. Zhang and J. Zhao, *Desalination*, **333**, 59 (2014).
43. M. F. G. Solomon, Y. Bhole and A. G. Livingston, *J. Macromol. Sci.*, **423**, 371 (2012).
44. D. H. N. Perera, Q. Song, H. Qiblawey and E. Sivaniah, *J. Membr. Sci.*, **487**, 74 (2015).
45. X. You, T. Ma, Y. Su, H. Wu, M. Wu, H. Cai, G. Sun and Zh. Jiang, *J. Membr. Sci.*, **540**, 454 (2017).
46. D. Emadzadeh, W. J. Lau, M. Rahbari-Sisakht, H. Ilbeygi, D. Rana, T. Matsuura and A. F. Ismail, *Chem. Eng. J.*, **281**, 243 (2015).
47. Y. Gong, Sh. Gao, Y. Tian, Y. Zhu, W. Fang, Zh. Wang and J. Jin, *J. Membr. Sci.*, **600**, 11784 (2020).
48. A. Cañas, M. J. Ariza and J. Benavente, *J. Membr. Sci.*, **183**, 135 (2001).
49. M. Ghanbari, D. Emadzadeh, W. J. Lau, T. Matsuura and A. F. Ismail, *RSC Adv.*, **5**, 21268 (2015).
50. H. Hoseinpour, M. Jahanshahi, M. Peyravi and A. Nozad, *J. Ind. Eng. Chem.*, **46**, 244 (2017).
51. X. Wu, R. W. Field, J. J. Wu and K. Zhang, *J. Membr. Sci.*, **540**, 251 (2017).
52. Z. Liu, H. Yu, G. Kang, X. Jie, Y. Jin and Y. Cao, *J. Membr. Sci.*, **497**, 485 (2016).
53. L. Shen, J. Zuo and Y. Wang, *J. Membr. Sci.*, **537**, 186 (2017).
54. B. Mi and M. Elimelech, *J. Membr. Sci.*, **320**, 292 (2008).